ACCOUNTS of chemical research

pubs.acs.org/accounts Article

Design Principles for Efficient and Stable Water Splitting Photoelectrocatalysts

John R. Hemmerling, Aarti Mathur, and Suljo Linic*

Cite This: *Acc. Chem. Res.* 2021, 54, 1992–2002 Read Online

ACCESS | Metrics & More | Article Recommendations

CONSPECTUS: Photoelectrochemical water splitting is a promising avenue for sustainable production of hydrogen used in the chemical industry and hydrogen fuel cells. The basic components of most photoelectrochemical water splitting systems are semiconductor light absorbers coupled to electrocatalysts, which perform the desired chemical reactions. A critical challenge for the design of these systems is the lack of stability for the majority of desired semiconductors under operating water splitting conditions. One strategy to address this issue is to protect the semiconductor by covering it with a stabilizing insulator layer, creating a metal−insulator−semiconductor (MIS) architecture, which has demonstrated improved stability. In addition to enhanced stability, the insulator layer may significantly affect the electron and hole transfer, which governs the recombination rates. Furthermore, the insertion of an insulator layer leads to the introduction of additional insulator/electrocatalyst and insulator/semiconductor interfaces. These interfaces can impact the system's performance significantly, and they need to be carefully engineered to optimize the efficiencies of MIS systems. In this Account, we describe our recent progress in shedding light on the critical role of the insulator and the interfaces on the performance of MIS systems. We discuss our findings by focusing on the concrete example of planar n-type Si protected by a HfO_2 insulator layer and coupled to a Ni or Ir electrocatalyst that performs the oxygen evolution reaction, one of the water splitting half-reactions. To improve our fundamental understanding of the insulator layer, we precisely control the HfO_2 insulator thickness using atomic layer deposition (ALD), and we perform a series of rigorous electrochemical experiments coupled with theory and modeling. We demonstrate that by tuning the insulator thickness, we can control the flux and recombination of photogenerated electrons and holes to optimize the generated photovoltage. Despite optimizing the thickness, we find that the maximum generated photovoltage in MIS systems is often significantly lower than the upper performance limit, i.e., there are additional losses in the system that could not be addressed by optimizing the insulator thickness. We identify the sources of these losses and describe strategies to minimize them by a combination of improving the semiconductor light absorption, removing nonidealities associated with interfacial defects, and finding alternative insulators with improved charge carrier selectivity. Finally, we quantify the improvements that can be obtained by implementing these specific strategies. Our collective work outlines strategies to analyze MIS systems, identify the sources of efficiency losses, and optimize the design to approach the fundamental performance limits. These general approaches are broadly applicable to photoelectrochemical materials that utilize sunlight to produce value-added chemicals.

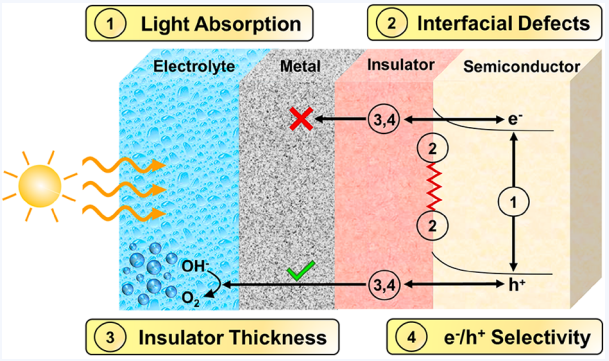

KEY REFERENCES

- Quinn, J.; Hemmerling, J.; Linic, S. Maximizing Solar Water Splitting Performance by Nanoscopic Control of the Charge Carrier Fluxes across Semiconductor−Electrocatalyst Junctions. *ACS Catal.* **2018**, *8*, 8545−8552.[1] *This study experimentally and computationally demonstrated significant photovoltage enhancements in metal−insulator−semiconductor (MIS) photoelectrocatalysts by precisely modulating the thickness of the insulator layer, which tunes the charge carrier fluxes and recombination. The studied MIS systems were Ni/HfO_2/n-Si performing the oxygen evolution reaction.*
- Hemmerling, J.; Quinn, J.; Linic, S. Quantifying Losses and Assessing the Photovoltage Limits in Metal−Insulator−Semiconductor Water Splitting Systems. *Adv. Energy Mater.* **2020**, *10*, 1903354.[2] *Using Ir/HfO_2/n-Si MIS systems as a case study, this work*

Received: January 29, 2021
Published: April 1, 2021

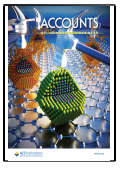

https://doi.org/10.1021/acs.accounts.1c00072
Acc. Chem. Res. 2021, 54, 1992−2002

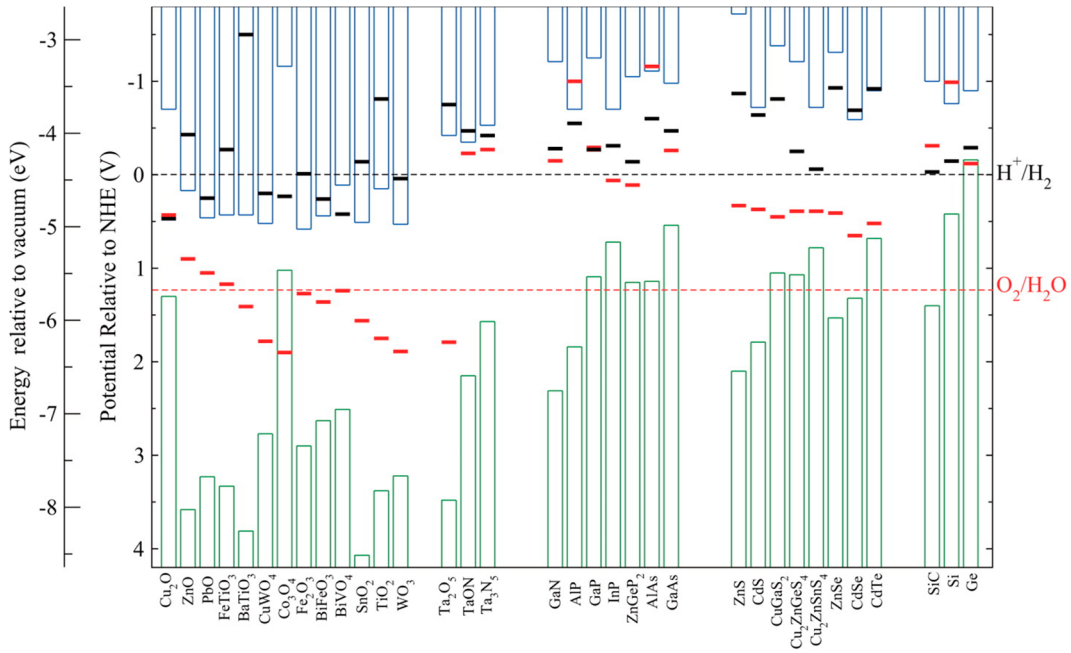

Figure 1. Properties of various semiconductors used for photocatalytic water splitting. The green and blue columns are the valence and conduction band edge positions, respectively. The red and black bars are the oxidation and reduction potentials of each semiconductor. Values are relative to the normal hydrogen electrode and the vacuum level for pH = 0, temperature of 298.15 K, and pressure of 1 bar. Under the water splitting conditions, the semiconductor will self-oxidize if the oxidation potential is above the OER redox potential and the semiconductor will self-reduce if the reduction potential is below the HER redox potential. Reproduced with permission from ref 9. Copyright 2012 American Chemical Society.

quantified the competing recombination mechanisms and the upper performance limits for MIS photoelectrocatalysts. Specifically, nonidealities from defects at the interfaces were demonstrated to result in significant losses.

- Quinn, J.; Hemmerling, J.; Linic, S. Guidelines for Optimizing the Performance of Metal−Insulator−Semiconductor (MIS) Photoelectrocatalytic Systems by Tuning the Insulator Thickness. *ACS Energy Lett.* **2019**, *4*, 2632−2638.[3] *This study explored bilayer-metal MIS photoelectrocatalysts in which the inner metal was optimized for generating photovoltage while the outer metal performed the hydrogen evolution reaction. The optimal insulator thickness was dependent on the junction properties of the inner metal.*
- Hernley, P. A.; Chavez, S. A.; Quinn, J. P.; Linic, S. Engineering the Optical and Catalytic Properties of Co-Catalyst/Semiconductor Photocatalysts. *ACS Photonics* **2017**, *4*, 979−985.[4] *This work demonstrated that embedding platinum nanoparticle electrocatalysts into a semiconductor rather than depositing them on the semiconductor's surface results in significantly improved light absorption and photoelectrocatalytic performance.*

INTRODUCTION

Materials that have received the most attention in photoelectrochemical water splitting consist of a light-absorbing semiconductor coupled to an attached metal electrocatalyst. In these water splitting systems, the semiconductor produces a photovoltage upon absorbing incident sunlight, and this voltage is used by respective electrocatalysts to drive the hydrogen evolution (HER) and oxygen evolution (OER) half-reactions. While the thermodynamic requirement to split water is 1.23 V, a minimum of ∼1.6 V is required when considering kinetic losses associated with the two half-reactions.[5]

Several studies have analyzed the optimal semiconductor band gaps required to achieve the necessary voltage to split water with high efficiency. Based on reasonable assumptions about the inherent efficiency losses, a single semiconductor photoelectrochemical system has a maximum solar-to-hydrogen (STH) efficiency of ∼12% for a band gap of ∼2.2 eV.[6,7] Similar analyses have shown that by using dual semiconductor light absorbers, the STH efficiencies can approach 25% for combinations of semiconductors with band gaps between 1 and 1.4 eV for the bottom absorber and between 1.7 and 2.1 eV for the top absorber.[6,7] Tandem systems can reach higher efficiencies because they absorb a higher fraction of the solar spectrum. These tandem systems are a promising approach to achieve the Department of Energy ultimate STH efficiency target of 25%.[8]

Data in Figure 1 show that there are many semiconductors that meet the band gap requirements for high efficiency tandem systems.[9] Among investigated systems, silicon (Si) with band gap of 1.1 eV is the prominent choice for the lower band gap semiconductor because of its earth abundance, low cost, and extensive commercial use.[10,11] A critical challenge in the application of Si and almost all semiconductors with desirable band gaps is their corrosion under water splitting conditions. Figure 1 shows the oxidation and reduction potentials for various semiconductors, suggesting that most semiconductors are not stable under the conditions of water splitting, i.e., there is a thermodynamic driving force to change their chemical and therefore optical (light absorption) properties.[9,12]

Over the past decade, it has been shown that oxide insulators can be introduced to protect some semiconductors against corrosion. In these systems, a stabilizing insulator layer is placed between a semiconductor and a metal-based electrocatalyst forming so-called metal−insulator−semicon-

https://doi.org/10.1021/acs.accounts.1c00072
Acc. Chem. Res. 2021, 54, 1992−2002

ductor (MIS) device architectures.[13,14] One of the first MIS water splitting systems used a TiO_2 insulator layer to stabilize Si.[15] Since this work, many protective insulators have been utilized in Si-based MIS photocatalysts, including Al_2O_3,[16−18] HfO_2,[1−3] SiO_2,[19−26] $SrTiO_3$,[27] TiO_2,[15,28−36] and ZrO_2.[37] The widespread deployment of these insulators was enabled by atomic layer deposition (ALD), which is a layer-by-layer growth technique to deposit conformal and pinhole-free layers of materials with sub-nanometer precision.[9,12,13,37−39]

In addition to improving stability, the incorporation of an insulator layer introduces additional factors, including the insulator thickness as well as metal−insulator and semiconductor−insulator interfaces, which can impact the overall system performance. A fundamental understanding of the impact of these factors on the performance of MIS photoelectrocatalysts is critical for their future development. In this Account, we discuss our recent work[1−3] where we combined modeling and experimental studies to shed light on the underlying mechanisms by which the introduction of an insulator affects water splitting performance. Specifically, we demonstrate the importance of (1) tuning the insulator thickness to modulate the recombination of electrons and holes, (2) minimizing interfacial defects, and (3) designing new insulators with improved charge transfer selectivity. In addition to the critical role of the insulator, we also discuss how the properties of the metal and semiconductor layers can be tuned to maximize performance and reach the practical limits. While this Account focuses on Si-based MIS photoelectrocatalysts for the OER, our approach and findings are broadly applicable to other photoelectrochemical devices.

PHOTOVOLTAGE AND RECOMBINATION

Figure 2 illustrates the equilibrium electronic structure of a metal/semiconductor (MS) system with a planar metal

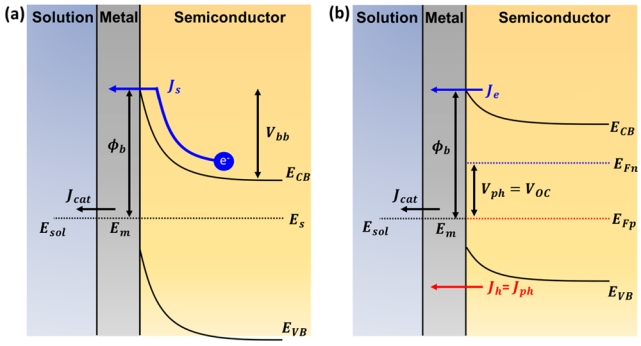

Figure 2. Energy band diagrams of a MS system with an n-type semiconductor and high work function metal immersed in an electrolyte. (a) System in the dark at equilibrium (V_a = 0, J_{net} = 0). The reverse saturation current (J_s) is governed by the barrier height (ϕ_b). (b) Illuminated system in quasi-equilibrium at the open-circuit potential (V_{oc}) such that there is no catalytic current ($J_{net} = J_{cat}$ = 0). The photovoltage ($V_{ph} = V_{oc}$) is defined by the splitting of the electron/hole quasi-Fermi levels (E_{fn}, E_{fp}).

electrocatalyst in direct contact with a planar n-type semiconductor in the dark and under illumination. Upon contact, electrons exchange between the metal, semiconductor, and electrolyte until their Fermi levels (E_m, E_s, and E_{sol}) are equilibrated. For the equilibration of an n-type semiconductor/metal interface, electrons will transfer from the semiconductor to the metal, leaving behind a positively charged depletion region. This charge redistribution leads to band bending in the semiconductor and an electric potential barrier (V_{bb} and ϕ_b in Figure 2a), which promotes the transport of holes and impedes the transport of electrons to the metal electrocatalyst. The electric potential barrier height (ϕ_b) reflects the difference between the metal work function (Fermi level, E_m) and the semiconductor conduction band edge (E_{cb}) (see Figure 2). Upon illumination, the MS system generates a photovoltage (V_{ph}), which is a critical performance metric for photoelectrocatalysts. The generated photovoltage is influenced by the flux of electrons (J_e) and holes (J_h) across the MS junction. In general, the relationship between photovoltage and the flux of charge carriers can be captured using the illuminated diode equation, which describes the net current (J_{net}) between the semiconductor and electrocatalyst as a function of voltage.

$$J_{net} = J_h + J_e = J_{ph} - J_s\left[\exp\left(-\frac{qV_a}{nkT}\right) - 1\right] \quad (1)$$

Here, J_{ph} is the photocurrent density, which is the total hole current (J_h) generated from solar absorption in the semiconductor. These holes ultimately drive the OER at the electrocatalyst. J_e is the electron current that reaches the metal by crossing the electric potential barrier. Since e^-/h^+ recombination in metals is very fast, this is essentially a recombination current. J_s is the dark saturation current, q is the elementary charge of an electron, V_a is the applied voltage defined as the difference between the semiconductor majority-carrier Fermi level and the solution Fermi level (this voltage can be applied using a potentiostat, and it is affected by the photovoltage generated upon illuminating the semiconductor), n is the ideality factor (n = 1 is ideal, n > 1 is nonideal), k is the Boltzmann constant, and T is temperature. J_s is a key parameter governing the electron current and therefore the e^-/h^+ recombination rates as well as the generated photovoltage. The expression for J_s depends on the system architecture. For MS systems with Si semiconductor, the dominant recombination mechanism is due to the recombination in the metal, and J_s can be analytically expressed by eq 2.[40]

$$J_s = A^*T^2 \exp\left(-\frac{q\phi_b}{kT}\right) \quad (2)$$

Here, A^* is Richardson's constant.

IMPACT OF THE INSULATOR

It has been widely demonstrated that eqs 1 and 2 capture the relationships between photogenerated current and voltage in MS systems. We wanted to understand how the introduction of a thin insulator between the metal and semiconductor impacts the performance. To answer this question, we fabricated Ni/HfO_2/n-Si MIS photoelectrocatalysts in which HfO_2 served as an insulator to protect n-Si under OER conditions. HfO_2 was deposited using ALD, and its thickness was manipulated by controlling the number of ALD cycles.[1] The photovoltage generated by the MIS system was measured as the voltage shift (evaluated at a current of 1 mA/cm^2) between the illuminated MIS system and an electrocatalyst control that employs the identical electrocatalyst. The data in Figure 3a show that photovoltage gradually increased as the HfO_2 thickness increased from 0 to 2.1 nm (0 to 22 ALD cycles) and decreased for thicker HfO_2. Specifically, tuning the HfO_2 thickness improves the photovoltage by 400 mV (up to ~480 mV) compared to the sample without HfO_2; that is, in

https://doi.org/10.1021/acs.accounts.1c00072
Acc. Chem. Res. 2021, 54, 1992−2002

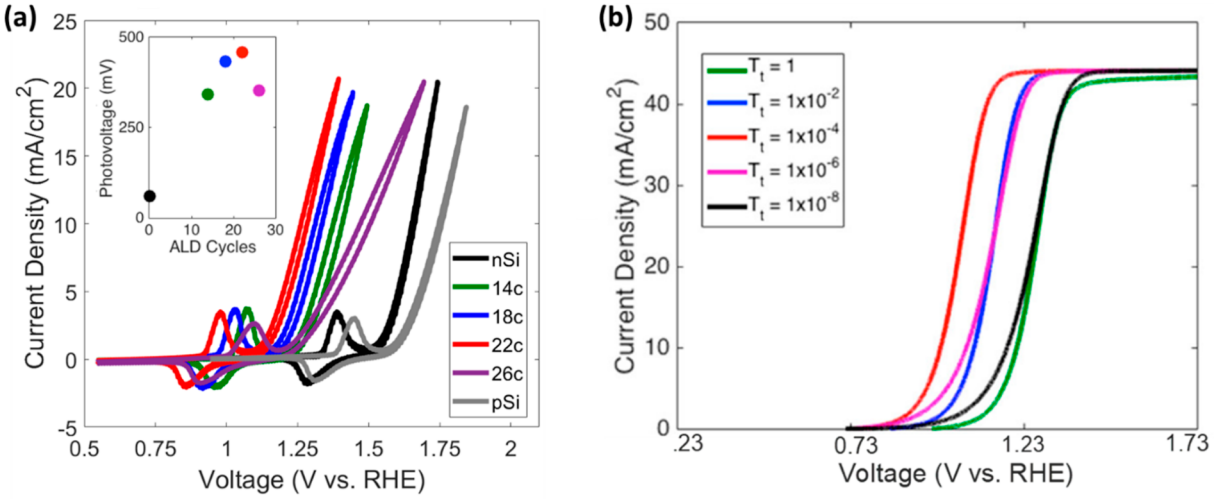

Figure 3. (a) Cyclic voltammetry in 1 M KOH of Ni/HfO_2/n-Si MIS systems with different HfO_2 thickness and a Ni/p-Si electrocatalyst control. The inset shows the photovoltage measured at 1 mA/cm^2 as a function of the HfO_2 thickness. (b) Modeled current−voltage response as a function of tunneling probability (HfO_2 thickness). Adapted with permission from ref 1. Copyright 2018 American Chemical Society.

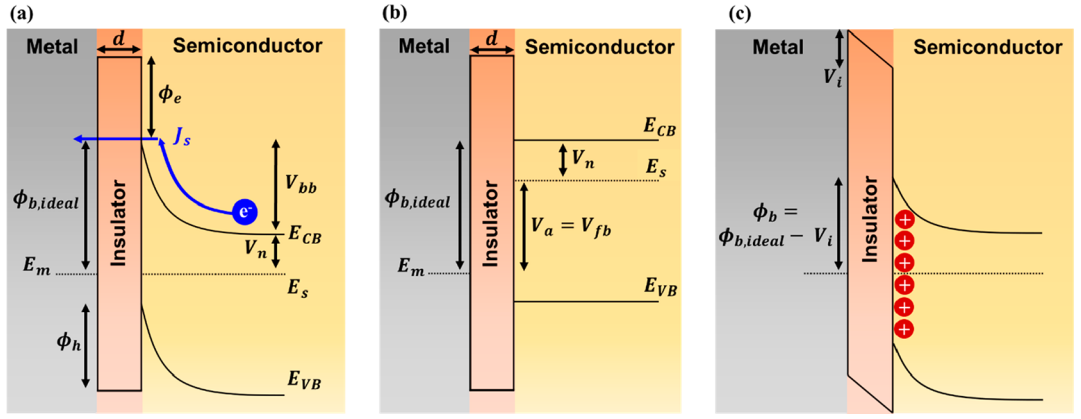

Figure 4. Energy band diagrams of a MIS system with an n-type semiconductor and high work function metal. (a) Ideal system (n = 1) in the dark at equilibrium (V_a = 0, J_{net} = 0). (b) Ideal system (n = 1) in the dark at the flat-band potential (V_a = V_{fb}). (c) Nonideal system (n > 1) with positively charged defects at the insulator/semiconductor interface. These defects cause an insulator voltage drop (V_i) which ultimately lowers the barrier height and photovoltage.

addition to improving the stability of the system, the insulator layer also improved the generated photovoltage.

To explain these results, we developed a comprehensive finite-difference time-domain (FDTD) model that iteratively solves the two governing equations for the transfer of charge carriers in these systems, Poisson's and the continuity equations.[1,3,41] The Butler−Volmer equation was employed to model the electrochemical OER rates (J_{cat} in Figure 2) as a function of the electrocatalyst voltage. An important boundary condition for this system of equations is the flux of charge carriers between the metal and semiconductor, which is influenced by the insulator. Since HfO_2 is a tunnel insulator, meaning that charge moves through the insulator via tunneling, we modeled the e^-/h^+ fluxes assuming the tunneling mechanism. Under this mechanism, when there is no insulator, the tunneling probability for the charge carriers is 1 (T_t = 1). As the thickness of the insulator increases, this probability drops according to the relationship $T_t = \exp(-\propto d\phi_e^{1/2})$, where $\propto$ is a constant that depends on the electron effective mass in the insulator, d is the insulator thickness, and ϕ_e is the offset between the semiconductor and insulator conduction bands (see Figure 4a for illustrations of these variables).[42] We used the same values for T_t for holes and electrons, which can be justified for n-Si/HfO_2 interfaces.[1]

The model outputs the current−voltage response of the system as a function of the tunneling probability and therefore the HfO_2 thickness (Figure 3b). The simulated current−voltage plots in Figure 3b qualitatively matched the experimental trends: the insulator layer with an intermediate tunneling probability (corresponding to ∼2.5 nm thick HfO_2) led to the optimal performance. The model allowed us to shed light on the mechanism responsible for the photovoltage enhancement of MIS photoelectrocatalysts with a particular insulator thickness. We found that in the limit of low insulator thickness (below ∼2.5 nm), the performance of the MIS system was limited by the large flux of electrons that can easily tunnel through the thin insulator to the electrocatalyst and recombine with the holes. On the other hand, for greater than 2.5 nm thickness, the electron recombination current becomes negligible; however, the hole current is impeded by the thicker insulator, which ultimately lowers the photovoltage. Overall, these initial modeling and experimental results demonstrate that by optimization of the insulator layer thickness, the e^-/h^+

https://doi.org/10.1021/acs.accounts.1c00072
Acc. Chem. Res. 2021, 54, 1992−2002

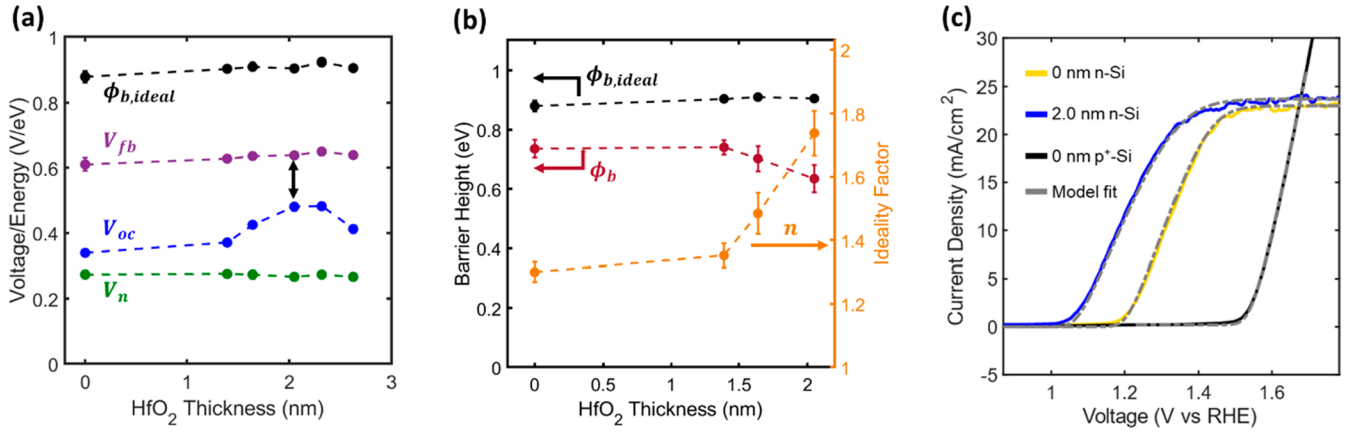

Figure 5. Compiled experimental results for Ir/HfO_2/n-Si photoelectrocatalysts with varied HfO_2 thickness. (a) Values for V_n, V_{fb}, and $\phi_{b,ideal}$ are obtained from Mott−Schottky plots and V_{oc} was determined by comparing to an Ir/p^+-Si electrocatalyst control. (b) n was obtained by measuring the performance as a function of light intensity, while ϕ_b was calculated from eq 8. (c) Experimental and modeled current−voltage plots demonstrate excellent agreement between experiment and modeling for Ir/2.0 nm HfO_2/n-Si, Ir/n-Si, and Ir/p^+-Si electrocatalytic control. Adapted with permission from ref 2. Copyright 2020 John Wiley and Sons.

fluxes can be optimized so that the recombination losses are minimized.

These studies demonstrated that the behavior of MIS systems (Figure 3a) can be captured by this rather complex system of equations that required numerical solutions (Figure 3b). We have also shown that in the limit of low insulator thickness (up to the ideal thickness), the system behavior can also be adequately described by a simpler analytical approach, where the diode equations (eqs 1 and 2) are augmented by recognizing that the insulator layer effectively serves as an additional barrier that decreases the electron dark saturation current (J_s). The expression for J_s in MIS systems is[42]

$$J_s = A^*T^2 \exp\left(-\frac{q\phi_b}{kT}\right)\exp(-\propto d\phi_e^{1/2}) \tag{3}$$

The second exponential term in eq 3 is the above-mentioned probability of electrons tunneling through an insulator layer. We reiterate that this expression can describe MIS systems in a thin insulator regime where the hole current (J_{ph} in eq 1) is not affected significantly by the insulator.[43]

An analytical expression for the photovoltage (V_{ph}) generated by a MIS system (in the limit of low insulator thickness) as a function of the net current (J_{net}) can be easily obtained by substituting eq 3 into eq 1,[1,2,17,42]

$$|V_{ph}| \approx \frac{nkT}{q}\left[\ln\frac{J_{ph}-J_{net}}{J_s}\right] = \frac{nkT}{q}\left[\ln\frac{J_{ph}-J_{net}}{A^*T^2} + \frac{q}{kT}\phi_b + \propto d\phi_e^{1/2}\right] \tag{4}$$

This expression is valid when $\frac{J_{ph}-J_{net}}{J_s} \gg 1$, which is met for essentially all relevant operating conditions. The maximum photovoltage is obtained when the net current is 0. This voltage is labeled as the open-circuit photovoltage ($V_{oc} = V_{ph}(J_{net} = 0)$). Equation 4 suggests that in addition to the properties of the insulator layer that affect the tunneling probability (d, ϕ_e), the photovoltage is also impacted by the ideality factor (n), the barrier height (ϕ_b), and the photocurrent (J_{ph}).

PERFORMANCE LIMITS AND NONIDEALITIES IN MIS PHOTOELECTROCATALYSTS

Following this initial work, we wanted to understand how the measured photovoltage compared to the fundamental performance limits of these MIS systems. In this context, it is also critical to quantify how, in addition to the above-discussed properties of the insulator layer (d, ϕ_e), other parameters in eq 4 (the ideality factor (n), the barrier height (ϕ_b), and the photocurrent (J_{ph})) impact the performance of MIS systems. To quantify these parameters, we performed studies using a MIS system consisting of Ir electrocatalysts on HfO_2/n-Si. The data in Figure 5a show the measured photovoltage for these Ir/HfO_2/n-Si photoelectrocatalysts as a function of insulator thickness.[2] Similar to the previous Ni-based MIS systems, the optimal HfO_2 thickness was 2.0 nm, yielding a photovoltage of ∼480 mV, which is ∼160 mV higher than Ir/n-Si samples without HfO_2.

The upper photovoltage limit for a MIS system is the flat-band potential (V_{fb}), which is also known as the built-in potential. This is the applied voltage or generated photovoltage required to reach the state where the semiconductor bands no longer bend (i.e., become flat, see Figure 4b). Assuming negligible contributions from the insulator, the flat-band potential is theoretically defined by the Fermi levels of the metal (E_m) and the semiconductor (E_s) (see Figure 4b):

$$V_{fb} = E_m - E_s \tag{5}$$

A common method to experimentally quantify the flat-band potential is based on the Mott−Schottky equation, which for an n-type semiconductor takes the following form:[2,44]

$$\left(\frac{1}{C_{sc}}\right)^2 = \frac{2}{\varepsilon_0\varepsilon_s A^2 q N_D}\left(V_a - V_{fb} - \frac{kT}{q}\right) \tag{6}$$

A, ε_0, and ε_s and are the surface area of the junction, vacuum permittivity, and semiconductor relative permittivity, respectively. By measuring the capacitance (C_{sc}) of the MIS system as a function of applied voltage (V_a), we can extract from eq 6 the flat-band potential and semiconductor doping density (N_D). The data in Figure 5a show that V_{fb} for all Ir/HfO_2/n-Si MIS samples was ∼630 mV; that is, the insulator layer thickness did not affect the flat-band potential in accordance with eq 5. This

https://doi.org/10.1021/acs.accounts.1c00072
Acc. Chem. Res. 2021, 54, 1992−2002

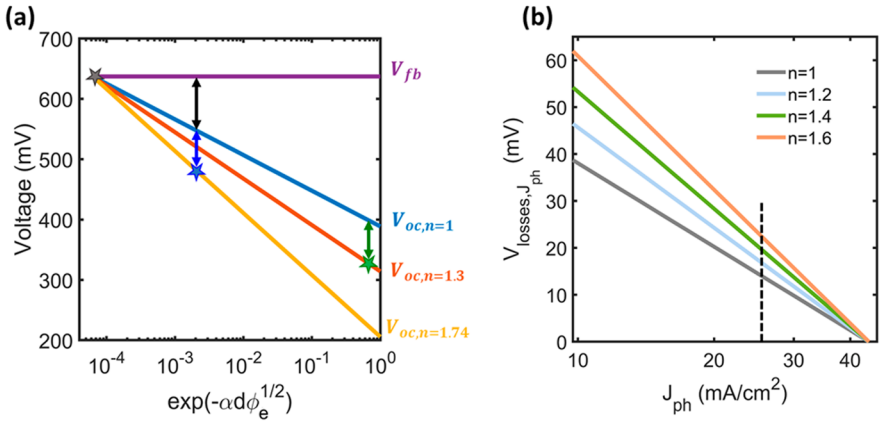

Figure 6. (a) Modeled (lines) and experimental (stars) photovoltages and flat-band potential as a function of the tunneling probability for the Ir/HfO_2/n-Si MIS samples. The model lines were obtained using eq 9 and the data from Figure 5. The blue star represents the experimental data point for the Ir/HfO_2/n-Si system with the optimal 2 nm HfO_2, and the green star represents the Ir/n-Si system without an insulator. The blue and green arrows correspond to the ∼70 mV V_{losses} associated with nonidealities in the system as described in the text. The black arrow represents additional V_{losses} totaling 80 mV. The gray star represents a system that achieves the photovoltage upper limit of the flat-band potential, which can be obtained if the tunnel probability is less than 0.0001 (assuming no changes to J_{ph}). (b) Modeled V_{losses} as a function of photocurrent and ideality factor. The dashed line represents the photocurrent observed experimentally for Ir/HfO_2/n-Si photoelectrocatalysts.

analysis showed that despite optimizing the insulator thickness, the maximum measured photovoltage of 480 mV is significantly lower than the flat-band potential; i.e., there was ∼150 mV of losses in the system that could not be addressed by tuning the insulator thickness.[2]

To understand why these systems fail to reach the upper performance limits, we analyzed the impact of the insulator on the barrier height and ideality factor, which also affect the photovoltage (eq 4). For an ideal system (n = 1), the ideal barrier height ($\phi_{b,ideal}$) can be determined from the flat-band potential (see Figure 4b):[45]

$$\phi_{b,ideal} = V_{fb} + V_n = V_{fb} + \frac{kT}{q}\ln\frac{N_C}{N_D} \quad (7)$$

Here, V_n is the offset between the semiconductor Fermi level and conduction band edge (see Figure 4a). It is a function of the doping density (N_D) and the effective density of states in the semiconductor conduction band (N_C). The values for $\phi_{b,ideal}$ and V_n can be computed, via eq 7, using the measured V_{fb} and N_D from the previous Mott−Schottky analysis. These are plotted in Figure 5a.

Compared to ideal systems, the presence of nonidealities (n > 1) causes the barrier height in MIS systems to be lower than the ideal barrier height according to the following expression:[2,45]

$$\phi_b = \frac{\phi_{b,ideal}}{n} + \left(\frac{n-1}{n}\right)V_n \quad (8)$$

We quantify the ideality factor for our Ir/HfO_2/n-Si systems by varying the light intensity (changing J_{ph}) and measuring the open-circuit photovoltage (V_{oc}).[2,20,25,26] Based on eq 4, a plot of V_{oc} vs ln(J_{ph}) yields a line with a slope that is related to the ideality factor and an intercept that is related to the dark saturation current (J_s).[2,17] The ideality factors measured using this approach as well as the resulting barrier height (calculated using eq 8) are reported in Figure 5b. The results demonstrate that there are significant nonidealities (n > 1) in these Ir/HfO_2/n-Si systems that lower the barrier height (ϕ_b) compared to the ideal value ($\phi_{b,ideal}$). For example, the sample with optimal photovoltage (2.0 nm HfO_2) exhibits an ideality factor of 1.74, yielding a barrier height of 0.63 eV, which is 0.27 eV lower than the ideal barrier height of 0.9 eV.

Although there are several possible sources of nonidealities, they are typically attributed to defects at the semiconductor/insulator interface in MIS systems.[2] These defects can result in significant charge build-up at the interface, which causes a voltage drop in the insulator (V_i in Figure 4c).[42] As illustrated in Figure 4c, the charge build-up lowers the barrier height relative to the ideal value as some of the voltage is lost as a voltage drop in the insulator (i.e., $\phi_b = \phi_{b,ideal} - V_i$).

We also modeled the current−voltage behavior of these Ir/HfO_2/n-Si photoelectrocatalysts performing OER. Here, we employed the Butler−Volmer equation to approximate the dark electrocatalytic reaction of the Ir/p^+-Si sample. We then used eqs 1, 3, and 8 with the experimentally measured ideality factors and barrier heights from Figure 5b to model the photovoltage as a function of current.[2] The data in Figure 5c show that the model closely matches the experimental data for samples with and without HfO_2.

QUANTIFYING LOSSES WITH A NEW METRIC: *V*losses

Given the presence of nonidealities and decreased barrier heights, it is desirable to quantify the extent to which these different factors impact the photovoltage losses. To quantify the losses, we introduce a new metric, V_{losses}, which is the difference between a system's flat-band potential (i.e., the upper photovoltage limit) and its generated open-circuit photovoltage. This difference will be zero for a system without losses (i.e., negligible recombination). The analytical expression for V_{losses} in MIS systems can be obtained by algebraic manipulation of eqs 4, 5, 7, and 8:

$$V_{losses} = V_{fb} - |V_{oc}| \approx \frac{nkT}{q}\left[\ln\left(\frac{A^*T^2}{J_{ph}}\right) - \frac{q}{kt}V_n - \propto d\phi_e^{1/2}\right] \quad (9)$$

The four main parameters that impact the performance of these systems are the photocurrent (J_{ph}), the properties of the

https://doi.org/10.1021/acs.accounts.1c00072
Acc. Chem. Res. 2021, 54, 1992−2002

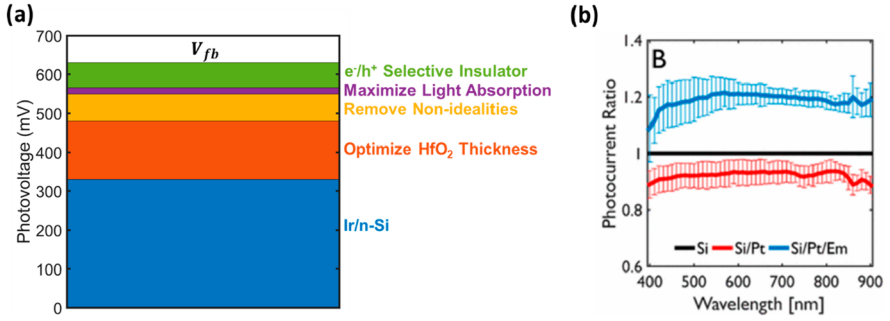

Figure 7. (a) Components that contribute to the photovoltage and the losses relative to the upper limit of the flat-band potential for the Ir/HfO_2/n-Si system. (b) Experimental photocurrent (relative to bare Si) for samples with Pt nanoparticles either deposited on the Si or embedded in the Si. Reproduced with permission from ref 4. Copyright 2017 American Chemical Society.

insulator (d and ϕ_e), the presence of nonidealities (n), and the semiconductor doping density (related to V_n). We note that the Richardson constant (A^*) is not a tunable parameter but is rather an inherent property for a given semiconductor.

Using eq 9, we can quantify the losses in MIS systems and suggest ways to achieve a photovoltage that approaches the upper limits. The data in Figure 6a show the photovoltage as a function of the insulator tunneling probability and the ideality factor for our Ir/HfO_2/n-Si systems as calculated using eq 9. The other parameters were measured as described above. The stars in the plot refer to the measured experimental data. The ideality factors of 1, 1.3, and 1.74 correspond to an ideal system, the experimental Ir/n-Si system (i.e., 0 nm HfO_2), and the experimental 2 nm HfO_2 system, respectively. For both, Ir/n-Si and Ir/2 nm-HfO_2/n-Si, the photovoltage losses associated with nonidealities (i.e., the difference between the performance of an ideal and a nonideal system) are ∼70 mV, as indicated by the blue and green arrows in Figure 6a. In other words, a photovoltage enhancement of ∼70 mV is possible by removing nonidealities from these MIS systems.

Figure 6a also shows that even if all nonidealities were eliminated (n = 1), the optimal thickness of 2 nm HfO_2 would generate a photovoltage that is still ∼80 mV below the flat-band potential (i.e., V_{losses} = 80 mV). Based on eq 9, the V_{losses} can theoretically be eliminated by using an insulator with a tunnel probability (T_t) less than 0.0001 (gray star in Figure 6a). This tunneling probability can be achieved with a HfO_2 layer of ∼3 nm; however, as we previously established, a thick HfO_2 insulator leads to additional photovoltage drops because the hole transport is impeded. This analysis suggests that HfO_2 may not be suitable to maximize photovoltage, and insulators with better selectivity toward hole transport compared to the electron transport are necessary to further improve the performance.

Besides the dominant role of the insulator physical thickness and tunneling probabilities as well as system nonidealities, there are also losses associated with the photocurrent and light absorption in the semiconductor (J_{ph} in eq 9). The maximum photocurrent that can be obtained for Si under 1-sun illumination is ∼44 mA/cm^2. However, parasitic light absorption and reflection from the catalyst layer significantly lowers the photocurrent. The photocurrent for our samples was ∼24 mA/cm^2, leading to photovoltage losses of 20−30 mV associated with the poor utilization of light (Figure 6b).

OUTLOOK AND FUTURE PROSPECTS

As described herein, there has been considerable interest in developing MIS photoelectrocatalysts throughout the past decade. The initial interest in the introduction of insulators was primarily driven by the desire to enhance the stability of various semiconductors under corrosive water splitting conditions. We have described our recent work aimed at shedding light on the connections between the introduction of an insulator and the performance of MIS systems. This work has allowed us to identify different parameters that play critical roles in the performance of these systems. Furthermore, through experimental measurements and modeling, we can identify the best approaches that can be employed to improve the performance of these systems. For example, our work on planar Ir/HfO_2/n-Si systems has shown that the introduction of a HfO_2 insulator and optimization of its thickness results in significantly increased photovoltage (in this case by ∼160 mV). We also learned that these increases in photovoltage are not sufficient to approach the upper performance limits of the flat-band potential (in this case, the maximum measured photovoltage was ∼150 mV lower than flat-band). We showed that these additional losses can be minimized by a combination of improving light absorption by the semiconductor (up to 30 mV under 1-sun illumination), removing nonidealities (up to 70 mV), and incorporating a different insulator with an improved carrier selectivity (up to 150 mV). Figure 7a illustrates the extent to which each of these factors can improve the photovoltage up to the flat-band potential.

It is critical to understand how to engineer MIS systems that can exhibit these improvements. In terms of maximizing light absorption in the semiconductor, there are several useful strategies such as texturing the surface, introducing an antireflection coating, and incorporating plasmonic metal nanoparticles.[23,25,26,32,46−51] For example, our group demonstrated that by embedding nanoparticle electrocatalysts in a semiconductor as opposed to dispersing them on the semiconductor's surface, the light reflection and parasitic light absorption by the metal are minimized.[4] In this particular example, 150 nm diameter Pt nanoparticles were embedded into p-type Si, and the system was analyzed for photoelectrochemical HER activity. As shown in Figure 7b, the embedded nanoparticle system increases the light-limited photocurrent by ∼24% compared to the nonembedded system and by ∼15% compared to bare Si. Furthermore, this strategy of embedding nanoparticles can introduce unique catalytic active sites. A fundamental understanding of the catalysis and

https://doi.org/10.1021/acs.accounts.1c00072
Acc. Chem. Res. 2021, 54, 1992−2002

measuring rates is another important focus in the literature.[52−54]

In addition to the management of light reflections and absorption, significant efforts need to focus on identifying the physical sources of nonidealities. In general, an insulator introduces additional interfaces, which are often sources of defect states that can result in significant charge build-up and a voltage drop in the insulator. The presence of these interfacial defect states will show up as a nonideality in the models discussed above. The common approaches to address these defects include annealing or chemical treatments aimed at removing the defect states.[2,28,34] In addition to interfacial defects, nonidealities can result from image force lowering, barrier height inhomogeneity, recombination in the semiconductor depletion region, and field emission.[2] While these nonidealities may be negligible for some MIS systems, including the ones discussed above, removing these sources of nonidealities would require alternative approaches for different systems.

Our results also show that systems incorporating an insulator with improved e^-/h^+ selectivity can generate photovoltages that approach the upper limits. To this end, novel insulators with better e^- or h^+ selectivity, depending on the desired half-reaction, should be explored. Indeed, this strategy has been implemented in high-efficiency photovoltaics, and the charge carrier selectivity may be improved by introducing dopant ions to the insulator or by utilizing alternative transition metal oxides such as MoO_x or V_2O_x.[55] We note that even with a perfectly selective insulator, the photovoltage may remain slightly below the flat-band potential as other recombination mechanisms (e.g., radiative recombination, Shockley−Read−Hall recombination, or recombination at the back contact) may become dominant and limit the performance.[2]

Despite the importance of the flat-band potential, only a few studies have explored methods to increase it. One way to achieve a higher flat-band potential is to increase the doping density of semiconductors, although one must be aware that the doping density can also influence the photocurrent and the minority carrier diffusion length.[2] Furthermore, if the doping density becomes too large, this can introduce alternative recombination pathways from field emission and Auger recombination.[40] The flat-band potential can also be increased by incorporating metals or metal oxides with high (for n-Si) and low (for p-Si) work functions.

We have discussed above the work on protecting and improving Si by introducing insulator layers. Moving forward, significant effort should be dedicated to implementation of MIS concepts to wider band gap semiconductors. Some groups have studied the performance of MIS architecture for Ni/TiO_2/$BiVO_4$[56] and graded MoS_x/c-TiO_2/$GaInP_2$[57] MIS systems; however, the important fundamental concepts of photovoltage, flat-band potential, and barrier height were not analyzed. p-Type Cu_2O (band gap ∼2.1 eV) is a suitable option for coupling with n-Si in a tandem configuration. Good performance has been achieved by forming pn heterojunctions, but MIS junctions with Cu_2O have not yet been demonstrated.[58]

More research should also focus on incorporating Si into practical tandem water splitting systems. So far, the STH efficiency of Si coupled to a wide band gap semiconductor in a tandem configuration is below 5%, and the semiconductors are electrically connected with wires.[59−63] A more integrated design consists of Si in direct contact with a wide band gap semiconductor. Attempts at fabricating fully integrated tandem structures utilizing Si have not generated enough voltage to split water[64−66] until very recently.[10,67] Important considerations for these integrated tandem systems are the design of the interfaces between the semiconductors and the light absorption and photocurrent matching between the semiconductors. Since Si is the bottom absorber in the tandem configuration, photons will enter the Si through the backside, and the high-energy photons will be preferentially absorbed by the wide-band gap semiconductor.[68] Thus, the photocurrent through Si in the tandem configuration will be significantly lower compared to 1-sun illumination used in experiments. We note that the lower photocurrent will modestly lower the photovoltage by ∼20 mV compared to a sample with 1-sun illumination (Figure 6b). The above discussions and results of our Account should help enable the overarching goal in the water splitting community to develop stable, efficient, and economical tandem solar water splitting systems.

AUTHOR INFORMATION

Corresponding Author

Suljo Linic − *Department of Chemical Engineering and Catalysis Science and Technology Institute, University of Michigan, Ann Arbor, Michigan 48109, United States;* orcid.org/0000-0003-2153-6755; Email: linic@umich.edu

Authors

John R. Hemmerling − *Department of Chemical Engineering and Catalysis Science and Technology Institute, University of Michigan, Ann Arbor, Michigan 48109, United States;* orcid.org/0000-0002-8271-2858

Aarti Mathur − *Department of Chemical Engineering and Catalysis Science and Technology Institute, University of Michigan, Ann Arbor, Michigan 48109, United States*

Complete contact information is available at: https://pubs.acs.org/10.1021/acs.accounts.1c00072

Notes

The authors declare no competing financial interest.

Biographies

John Hemmerling received his B.S. in chemical engineering from Purdue University in 2016 and a M.S. in chemical engineering from the University of Michigan in 2018. He is currently pursuing a Ph.D. in chemical engineering at University of Michigan, working in the Linic lab. In 2017, John received a National Defense Science and Engineering Graduate Fellowship to aid his research in photoelectrochemical water splitting.

Aarti Mathur received her B.S. in chemical engineering from the Georgia Institute of Technology in 2019. She is currently pursuing a Ph.D. in chemical engineering at University of Michigan, working in the Linic lab. In 2021, Aarti was offered a National Science Foundation Fellowship and a National Defense Science and Engineering Graduate Fellowship based on her research in photoelectrochemical water splitting.

Suljo Linic received his Ph.D. degree in chemical engineering at the University of Delaware in 2004 after receiving his B.S. degree in Physics with a minor in Mathematics and Chemistry from West Chester University in West Chester (PA). He was a Max Planck

https://doi.org/10.1021/acs.accounts.1c00072
Acc. Chem. Res. 2021, 54, 1992−2002

postdoctoral fellow at the theory department at the Fritz Haber Institute of Max Planck Society in Berlin (Germany). He is currently the Martin Lewis Perl Collegiate Professor of Chemical Engineering at the University of Michigan in Ann Arbor. He has also held an appointment as a Hans Fischer Fellow at the chemistry department of the Technical University Munich. His work focuses on light−matter interactions, photoelectrocatalysis, electrocatalysis, and thermal catalysis.

■ ACKNOWLEDGMENTS

This research was supported by the U.S. Department of Energy, Office of Science, Office of Basic Energy Sciences, under Award DE-SC0021362 (experimental work) and National Science Foundation (NSF, CBET-1803991) (modeling work). Secondary support for the development of analytical tools used in the model was provided by NSF (CBET-1702471 and CHE-1800197).

■ REFERENCES

(1) Quinn, J.; Hemmerling, J.; Linic, S. Maximizing Solar Water Splitting Performance by Nanoscopic Control of the Charge Carrier Fluxes across Semiconductor−Electrocatalyst Junctions. *ACS Catal.* **2018**, *8*, 8545−8552.

(2) Hemmerling, J.; Quinn, J.; Linic, S. Quantifying Losses and Assessing the Photovoltage Limits in Metal−Insulator−Semiconductor Water Splitting Systems. *Adv. Energy Mater.* **2020**, *10*, 1903354.

(3) Quinn, J.; Hemmerling, J.; Linic, S. Guidelines for Optimizing the Performance of Metal−Insulator−Semiconductor (MIS) Photoelectrocatalytic Systems by Tuning the Insulator Thickness. *ACS Energy Lett.* **2019**, *4*, 2632−2638.

(4) Hernley, P. A.; Chavez, S. A.; Quinn, J. P.; Linic, S. Engineering the Optical and Catalytic Properties of Co-Catalyst/Semiconductor Photocatalysts. *ACS Photonics* **2017**, *4*, 979−985.

(5) Walter, M. G.; Warren, E. L.; McKone, J. R.; Boettcher, S. W.; Mi, Q.; Santori, E. A.; Lewis, N. S. Solar Water Splitting Cells. *Chem. Rev.* **2010**, *110*, 6446−6473.

(6) Seitz, L. C.; Chen, Z.; Forman, A. J.; Pinaud, B. A.; Benck, J. D.; Jaramillo, T. F. Modeling Practical Performance Limits of Photoelectrochemical Water Splitting Based on the Current State of Materials Research. *ChemSusChem* **2014**, *7*, 1372−1385.

(7) Prévot, M. S.; Sivula, K. Photoelectrochemical Tandem Cells for Solar Water Splitting. *J. Phys. Chem. C* **2013**, *117*, 17879−17893.

(8) DOE Technical Targets for Hydrogen Production from Photoelectrochemical Water Splitting https://www.energy.gov/eere/fuelcells/doe-technical-targets-hydrogen-production-photoelectrochemical-water-splitting (accessed Dec 14, 2020).

(9) Chen, S.; Wang, L.-W. Thermodynamic Oxidation and Reduction Potentials of Photocatalytic Semiconductors in Aqueous Solution. *Chem. Mater.* **2012**, *24*, 3659−3666.

(10) Luo, Z.; Wang, T.; Gong, J. Single-Crystal Silicon-Based Electrodes for Unbiased Solar Water Splitting: Current Status and Prospects. *Chem. Soc. Rev.* **2019**, *48*, 2158−2181.

(11) Fan, R.; Mi, Z.; Shen, M. Silicon Based Photoelectrodes for Photoelectrochemical Water Splitting. *Opt. Express* **2019**, *27*, A51−A80.

(12) Bae, D.; Seger, B.; Vesborg, P. C. K.; Hansen, O.; Chorkendorff, I. Strategies for Stable Water Splitting via Protected Photoelectrodes. *Chem. Soc. Rev.* **2017**, *46*, 1933−1954.

(13) Scheuermann, A. G.; McIntyre, P. C. Atomic Layer Deposited Corrosion Protection: A Path to Stable and Efficient Photoelectrochemical Cells. *J. Phys. Chem. Lett.* **2016**, *7*, 2867−2878.

(14) Thalluri, S. M.; Bai, L.; Lv, C.; Huang, Z.; Hu, X.; Liu, L. Strategies for Semiconductor/Electrocatalyst Coupling toward Solar-Driven Water Splitting. *Advanced Science* **2020**, *7*, 1902102.

(15) Chen, Y. W.; Prange, J. D.; Dühnen, S.; Park, Y.; Gunji, M.; Chidsey, C. E. D.; McIntyre, P. C. Atomic Layer-Deposited Tunnel Oxide Stabilizes Silicon Photoanodes for Water Oxidation. *Nat. Mater.* **2011**, *10*, 539−544.

(16) Park, M.-J.; Jung, J.-Y.; Shin, S.-M.; Song, J.-W.; Nam, Y.-H.; Kim, D.-H.; Lee, J.-H. Photoelectrochemical Oxygen Evolution Improved by a Thin Al2O3 Interlayer in a NiOx/n-Si Photoanode. *Thin Solid Films* **2016**, *599*, 54−58.

(17) Digdaya, I. A.; Trześniewski, B. J.; Adhyaksa, G. W. P.; Garnett, E. C.; Smith, W. A. General Considerations for Improving Photovoltage in Metal−Insulator−Semiconductor Photoanodes. *J. Phys. Chem. C* **2018**, *122*, 5462−5471.

(18) Luo, Z.; Liu, B.; Li, H.; Chang, X.; Zhu, W.; Wang, T.; Gong, J. Multifunctional Nickel Film Protected N-Type Silicon Photoanode with High Photovoltage for Efficient and Stable Oxygen Evolution Reaction. *Small Methods* **2019**, *3*, 1900212.

(19) Mikolasek, M.; Frohlich, K.; Husekova, K.; Racko, J.; Rehacek, V.; Chymo, F.; Tapajna, M.; Harmatha, L. Silicon Based MIS Photoanode for Water Oxidation: A Comparison of RuO2 and Ni Schottky Contacts. *Appl. Surf. Sci.* **2018**, *461*, 48−53.

(20) Hill, J. C.; Landers, A. T.; Switzer, J. A. An Electrodeposited Inhomogeneous Metal−Insulator−Semiconductor Junction for Efficient Photoelectrochemical Water Oxidation. *Nat. Mater.* **2015**, *14*, 1150−1155.

(21) Oh, S.; Jung, S.; Lee, Y. H.; Song, J. T.; Kim, T. H.; Nandi, D. K.; Kim, S.-H.; Oh, J. Hole-Selective CoOx/SiOx/Si Heterojunctions for Photoelectrochemical Water Splitting. *ACS Catal.* **2018**, *8*, 9755−9764.

(22) Esposito, D. V.; Levin, I.; Moffat, T. P.; Talin, A. A. H_2 Evolution at Si-Based Metal−Insulator−Semiconductor Photoelectrodes Enhanced by Inversion Channel Charge Collection and H Spillover. *Nat. Mater.* **2013**, *12*, 562−568.

(23) Ji, L.; Hsu, H.-Y.; Li, X.; Huang, K.; Zhang, Y.; Lee, J. C.; Bard, A. J.; Yu, E. T. Localized Dielectric Breakdown and Antireflection Coating in Metal−Oxide−Semiconductor Photoelectrodes. *Nat. Mater.* **2017**, *16*, 127−131.

(24) Loget, G.; Mériadec, C.; Dorcet, V.; Fabre, B.; Vacher, A.; Fryars, S.; Ababou-Girard, S. Tailoring the Photoelectrochemistry of Catalytic Metal-Insulator-Semiconductor (MIS) Photoanodes by a Dissolution Method. *Nat. Commun.* **2019**, *10*, 3522.

(25) Esposito, D. V.; Lee, Y.; Yoon, H.; Haney, P. M.; Labrador, N. Y.; Moffat, T. P.; Talin, A. A.; Szalai, V. A. Deconvoluting the Influences of 3D Structure on the Performance of Photoelectrodes for Solar-Driven Water Splitting. *Sustainable Energy & Fuels* **2017**, *1*, 154−173.

(26) Lim, S. Y.; Ha, K.; Ha, H.; Lee, S. Y.; Jang, M. S.; Choi, M.; Chung, T. D. Three-Dimensionally Patterned Ag−Pt Alloy Catalyst on Planar Si Photocathodes for Photoelectrochemical H 2 Evolution. *Phys. Chem. Chem. Phys.* **2019**, *21*, 4184−4192.

(27) Ji, L.; McDaniel, M. D.; Wang, S.; Posadas, A. B.; Li, X.; Huang, H.; Lee, J. C.; Demkov, A. A.; Bard, A. J.; Ekerdt, J. G.; Yu, E. T. A Silicon-Based Photocathode for Water Reduction with an Epitaxial $SrTiO_3$ Protection Layer and a Nanostructured Catalyst. *Nat. Nanotechnol.* **2015**, *10*, 84−90.

(28) Scheuermann, A. G.; Lawrence, J. P.; Meng, A. C.; Tang, K.; Hendricks, O. L.; Chidsey, C. E. D.; McIntyre, P. C. Titanium Oxide Crystallization and Interface Defect Passivation for High Performance Insulator-Protected Schottky Junction MIS Photoanodes. *ACS Appl. Mater. Interfaces* **2016**, *8*, 14596−14603.

(29) Scheuermann, A. G.; Lawrence, J. P.; Kemp, K. W.; Ito, T.; Walsh, A.; Chidsey, C. E. D.; Hurley, P. K.; McIntyre, P. C. Design Principles for Maximizing Photovoltage in Metal-Oxide-Protected Water-Splitting Photoanodes. *Nat. Mater.* **2016**, *15*, 99−105.

(30) Jung, J.-Y.; Kim, D. W.; Park, T. J.; Lee, J.-H. Design Guidelines of Insulator for Improving Stability and Performance of Nano-electrocatalyst/Insulator/Semiconductor Photoelectrochemical Cells. *ACS Appl. Energy Mater.* **2020**, *3*, 1046−1053.

(31) Siddiqi, G.; Luo, Z.; Xie, Y.; Pan, Z.; Zhu, Q.; Röhr, J. A.; Cha, J. J.; Hu, S. Stable Water Oxidation in Acid Using Manganese-Modified TiO2 Protective Coatings. *ACS Appl. Mater. Interfaces* **2018**, *10*, 18805−18815.

https://doi.org/10.1021/acs.accounts.1c00072
Acc. Chem. Res. 2021, 54, 1992−2002

(32) Chen, C.-J.; Veeramani, V.; Wu, Y.-H.; Jena, A.; Yin, L.-C.; Chang, H.; Hu, S.-F.; Liu, R.-S. Phosphorous-Doped Molybdenum Disulfide Anchored on Silicon as an Efficient Catalyst for Photoelectrochemical Hydrogen Generation. *Appl. Catal., B* **2020**, *263*, 118259.
(33) Zheng, J.; Lyu, Y.; Wang, R.; Xie, C.; Zhou, H.; Jiang, S. P.; Wang, S. Crystalline TiO 2 Protective Layer with Graded Oxygen Defects for Efficient and Stable Silicon-Based Photocathode. *Nat. Commun.* **2018**, *9*, 3572.
(34) Chuang, C.-H.; Lai, Y.-Y.; Hou, C.-H.; Cheng, Y.-J. Annealed Polycrystalline TiO2 Interlayer of the N-Si/TiO2/Ni Photoanode for Efficient Photoelectrochemical Water Splitting. *ACS Appl. Energy Mater.* **2020**, *3*, 3902−3908.
(35) Choi, S.; Lee, S. A.; Yang, H.; Lee, T. H.; Kim, C.; Lee, C. W.; Shin, H.; Jang, H. W. Stabilization of NiFe Layered Double Hydroxides on N-Si by an Activated TiO2 Interlayer for Efficient Solar Water Oxidation. *ACS Appl. Energy Mater.* **2020**, *3*, 12298−12307.
(36) Yang, W.; Moehl, T.; Service, E.; Tilley, S. D. Operando Analysis of Semiconductor Junctions in Multi-Layered Photocathodes for Solar Water Splitting by Impedance Spectroscopy. *Adv. Energy Mater.* **2021**, *11*, 2003569.
(37) Cai, Q.; Hong, W.; Jian, C.; Li, J.; Liu, W. Insulator Layer Engineering toward Stable Si Photoanode for Efficient Water Oxidation. *ACS Catal.* **2018**, *8*, 9238−9244.
(38) Yang, W.; Prabhakar, R. R.; Tan, J.; Tilley, S. D.; Moon, J. Strategies for Enhancing the Photocurrent, Photovoltage, and Stability of Photoelectrodes for Photoelectrochemical Water Splitting. *Chem. Soc. Rev.* **2019**, *48*, 4979−5015.
(39) Cao, S.; Zhang, Z.; Liao, Q.; Kang, Z.; Zhang, Y. Interface Engineering for High-Performance Photoelectrochemical Cells via Atomic Layer Deposition Technique. *Energy Technol.* **2021**, *9*, 2000819.
(40) Rhoderick, E. H. Metal-Semiconductor Contacts. *IEE Proc., Part I: Solid-State Electron Devices* **1982**, *129*, 1.
(41) Mills, T. J.; Lin, F.; Boettcher, S. W. Theory and Simulations of Electrocatalyst-Coated Semiconductor Electrodes for Solar Water Splitting. *Phys. Rev. Lett.* **2014**, *112*, 148304.
(42) Card, H. C.; Rhoderick, E. H. Studies of Tunnel MOS Diodes I. Interface Effects in Silicon Schottky Diodes. *J. Phys. D: Appl. Phys.* **1971**, *4*, 1589.
(43) Liu, X. X.; Sites, J. R. Solar-cell Collection Efficiency and Its Variation with Voltage. *J. Appl. Phys.* **1994**, *75*, 577−581.
(44) Hankin, A.; Bedoya-Lora, F. E.; Alexander, J. C.; Regoutz, A.; Kelsall, G. H. Flat Band Potential Determination: Avoiding the Pitfalls. *J. Mater. Chem. A* **2019**, *7*, 26162−26176.
(45) Wagner, L. F.; Young, R. W.; Sugerman, A. A Note on the Correlation between the Schottky-Diode Barrier Height and the Ideality Factor as Determined from I-V Measurements. *IEEE Electron Device Lett.* **1983**, *4*, 320−322.
(46) Hong, W.; Cai, Q.; Ban, R.; He, X.; Jian, C.; Li, J.; Li, J.; Liu, W. High-Performance Silicon Photoanode Enhanced by Gold Nanoparticles for Efficient Water Oxidation. *ACS Appl. Mater. Interfaces* **2018**, *10*, 6262−6268.
(47) Hernley, P. A.; Linic, S. Modeling the Impact of Metallic Plasmonic Resonators on the Solar Conversion Efficiencies of Semiconductor Photoelectrodes: When Does Introducing Buried Plasmonic Nanostructures Make Sense? *J. Phys. Chem. C* **2018**, *122*, 24279−24286.
(48) Ingram, D. B.; Linic, S. Water Splitting on Composite Plasmonic-Metal/Semiconductor Photoelectrodes: Evidence for Selective Plasmon-Induced Formation of Charge Carriers near the Semiconductor Surface. *J. Am. Chem. Soc.* **2011**, *133*, 5202−5205.
(49) Chavez, S.; Rao, V. G.; Linic, S. Unearthing the Factors Governing Site Specific Rates of Electronic Excitations in Multicomponent Plasmonic Systems and Catalysts. *Faraday Discuss.* **2019**, *214*, 441−453.
(50) Linic, S.; Aslam, U.; Boerigter, C.; Morabito, M. Photochemical Transformations on Plasmonic Metal Nanoparticles. *Nat. Mater.* **2015**, *14*, 567−576.
(51) Linic, S.; Chavez, S.; Elias, R. Flow and Extraction of Energy and Charge Carriers in Hybrid Plasmonic Nanostructures. *Nat. Mater.* **2021**, DOI: 10.1038/s41563-020-00858-4.
(52) Dix, S. T.; Lu, S.; Linic, S. Critical Practices in Rigorously Assessing the Inherent Activity of Nanoparticle Electrocatalysts. *ACS Catal.* **2020**, *10*, 10735−10741.
(53) Cleve, T. V.; Moniri, S.; Belok, G.; More, K. L.; Linic, S. Nanoscale Engineering of Efficient Oxygen Reduction Electrocatalysts by Tailoring the Local Chemical Environment of Pt Surface Sites. *ACS Catal.* **2017**, *7*, 17−24.
(54) Dix, S. T.; Linic, S. In-Operando Surface-Sensitive Probing of Electrochemical Reactions on Nanoparticle Electrocatalysts: Spectroscopic Characterization of Reaction Intermediates and Elementary Steps of Oxygen Reduction Reaction on Pt. *J. Catal.* **2021**, *396*, 32−39.
(55) Gao, P.; Yang, Z.; He, J.; Yu, J.; Liu, P.; Zhu, J.; Ge, Z.; Ye, J. Dopant-Free and Carrier-Selective Heterocontacts for Silicon Solar Cells: Recent Advances and Perspectives. *Advanced Science* **2018**, *5*, 1700547.
(56) McDowell, M. T.; Lichterman, M. F.; Spurgeon, J. M.; Hu, S.; Sharp, I. D.; Brunschwig, B. S.; Lewis, N. S. Improved Stability of Polycrystalline Bismuth Vanadate Photoanodes by Use of Dual-Layer Thin TiO2/Ni Coatings. *J. Phys. Chem. C* **2014**, *118*, 19618−19624.
(57) Gu, J.; Aguiar, J. A.; Ferrere, S.; Steirer, K. X.; Yan, Y.; Xiao, C.; Young, J. L.; Al-Jassim, M.; Neale, N. R.; Turner, J. A. A Graded Catalytic−Protective Layer for an Efficient and Stable Water-Splitting Photocathode. *Nature Energy* **2017**, *2*, 16192.
(58) Cendula, P.; Mayer, M. T.; Luo, J.; Grätzel, M. Elucidation of Photovoltage Origin and Charge Transport in Cu2O Heterojunctions for Solar Energy Conversion. *Sustainable Energy Fuels* **2019**, *3*, 2633−2641.
(59) Vijselaar, W.; Westerik, P.; Veerbeek, J.; Tiggelaar, R. M.; Berenschot, E.; Tas, N. R.; Gardeniers, H.; Huskens, J. Spatial Decoupling of Light Absorption and Catalytic Activity of Ni−Mo-Loaded High-Aspect-Ratio Silicon Microwire Photocathodes. *Nature Energy* **2018**, *3*, 185−192.
(60) Feng, S.; Wang, T.; Liu, B.; Hu, C.; Li, L.; Zhao, Z.-J.; Gong, J. Enriched Surface Oxygen Vacancies of Photoanodes by Photoetching with Enhanced Charge Separation. *Angew. Chem., Int. Ed.* **2020**, *59*, 2044−2048.
(61) Jang, J.-W.; Du, C.; Ye, Y.; Lin, Y.; Yao, X.; Thorne, J.; Liu, E.; McMahon, G.; Zhu, J.; Javey, A.; Guo, J.; Wang, D. Enabling Unassisted Solar Water Splitting by Iron Oxide and Silicon. *Nat. Commun.* **2015**, *6*, 7447.
(62) Liu, B.; Feng, S.; Yang, L.; Li, C.; Luo, Z.; Wang, T.; Gong, J. Bifacial Passivation of n -Silicon Metal−Insulator−Semiconductor Photoelectrodes for Efficient Oxygen and Hydrogen Evolution Reactions. *Energy Environ. Sci.* **2020**, *13*, 221−228.
(63) Xu, P.; Feng, J.; Fang, T.; Zhao, X.; Li, Z.; Zou, Z. Photoelectrochemical Cell for Unassisted Overall Solar Water Splitting Using a BiVO 4 Photoanode and Si Nanoarray Photocathode. *RSC Adv.* **2016**, *6*, 9905−9910.
(64) Kunturu, P. P.; Zachariadis, C.; Witczak, L.; Nguyen, M. D.; Rijnders, G.; Huskens, J. Tandem Si Micropillar Array Photocathodes with Conformal Copper Oxide and a Protection Layer by Pulsed Laser Deposition. *ACS Appl. Mater. Interfaces* **2019**, *11*, 41402−41414.
(65) Vijselaar, W.; Kunturu, P. P.; Moehl, T.; Tilley, S. D.; Huskens, J. Tandem Cuprous Oxide/Silicon Microwire Hydrogen-Evolving Photocathode with Photovoltage Exceeding 1.3 V. *ACS Energy Lett.* **2019**, *4*, 2287−2294.
(66) Shaner, M. R.; Fountaine, K. T.; Ardo, S.; Coridan, R. H.; Atwater, H. A.; Lewis, N. S. Photoelectrochemistry of Core−Shell Tandem Junction n−p + -Si/n-WO 3 Microwire Array Photoelectrodes. *Energy Environ. Sci.* **2014**, *7*, 779−790.

https://doi.org/10.1021/acs.accounts.1c00072
Acc. Chem. Res. 2021, 54, 1992−2002

(67) Vanka, S.; Zhou, B.; Awni, R. A.; Song, Z.; Chowdhury, F. A.; Liu, X.; Hajibabaei, H.; Shi, W.; Xiao, Y.; Navid, I. A.; Pandey, A.; Chen, R.; Botton, G. A.; Hamann, T. W.; Wang, D.; Yan, Y.; Mi, Z. InGaN/Si Double-Junction Photocathode for Unassisted Solar Water Splitting. *ACS Energy Lett.* **2020**, *5*, 3741−3751.
(68) Bae, D.; Pedersen, T.; Seger, B.; Malizia, M.; Kuznetsov, A.; Hansen, O.; Chorkendorff, I.; Vesborg, P. C. K. Back-Illuminated Si Photocathode: A Combined Experimental and Theoretical Study for Photocatalytic Hydrogen Evolution. *Energy Environ. Sci.* **2015**, *8*, 650−660.

https://doi.org/10.1021/acs.accounts.1c00072
Acc. Chem. Res. 2021, 54, 1992−2002